Modern Pathology (2019) 32:1536–1543
https://doi.org/10.1038/s41379-019-0292-y

ARTICLE

Histological differences in cancer cells, stroma, and luminal spaces strongly correlate with in vivo MRI-detectability of prostate cancer

Kosuke Miyai[1,2] · Ayako Mikoshi[3] · Fumiko Hamabe[3] · Kuniaki Nakanishi[2] · Keiichi Ito[4] · Hitoshi Tsuda[1] · Hiroshi Shinmoto[3]

Received: 4 February 2019 / Revised: 27 April 2019 / Accepted: 27 April 2019 / Published online: 7 June 2019

Abstract

The current study aimed to investigate the plausible histopathological factors that affect the detectability of prostate cancers on multiparametric magnetic resonance imaging (MP-MRI). This retrospective study included 59 consecutive patients who had undergone MP-MRI and subsequent radical prostatectomy. The cases were standardized according to the tumor size ranging from 10 to 20 mm on the final pathological diagnosis. Histopathological review and semi-automated imaging analysis were performed to evaluate the relative area fractions of the histological components, including cancer cells, stroma, and luminal spaces. Among the 59 prostatectomy specimens, no case showed two or more foci of cancer that matched the size criteria. Of the 59 lesions, 35 were MRI-detectable [Prostate Imaging Reporting and Data System (PIRADS) score of 3 or greater] and 24 were MRI-undetectable (PIRADS score of 2 or less). No significant differences were observed in Gleason Grade Group, percentage of Gleason pattern 4, and predominant subtype of Gleason pattern 4 between MRI-detectable and MRI-undetectable cancers. On the other hand, significantly higher mean area fraction of cancer cells (60.9% vs. 42.7%, $P < 0.0001$) and lower mean area fractions of stroma (33.8% vs. 45.1%, $P = 0.00089$) and luminal spaces (5.2% vs. 12.2%, $P < 0.0001$) were observed in MRI-detectable cancers than in MRI-undetectable cancers. In a multivariable analysis performed upon exclusion of area fraction of stroma due to its multicollinearity with that of cancer cells, area fractions of cancer cells ($P = 0.0031$) and luminal space ($P = 0.0035$) demonstrated strong positive and negative correlation with MRI-detectability, respectively. Changes in cancer cells, stroma, and luminal spaces, rather than conventional histological parameters, could be considered one of the best predictors to clinical, in vivo MRI-detectability of prostate cancer.

Introduction

The current standard of screening for prostate cancer relies on measurement of the levels of prostate-specific antigen (PSA) and digital rectal examination followed by systematic transrectal ultrasonography-guided biopsy (TRUS-biopsy) during which 10 to 12 cores are obtained. In 2014, the International Society of Urological Pathology (ISUP) and the World Health Organization (WHO) approved a new grading system of prostate cancer, which is more accurate for predicting cancer specific mortality than the traditional Gleason scoring system [1]. Pathologically significant cancer is generally defined as a cancer focus of Grade Group 2 (i.e., Gleason score 3+4) or greater, which is based on the evidence that cancers with Grade Group 1 (i.e., Gleason score 3+3) are clinically indolent with no significant difference in the rate of mortality of patients between groups treated with surgery and observation only [2–4]. From this viewpoint, the traditional approach is associated with under-detection of clinically significant cancers and over-detection of clinically insignificant cancers [5].

Recently, multiparametric magnetic resonance imaging (MP-MRI) has emerged as a useful diagnostic device in the detection, localization, and risk assessment of prostate cancer. A large amount of evidence indicates that targeted

✉ Kosuke Miyai
mykusu228@nifty.com

[1] Department of Basic Pathology, National Defense Medical College, Tokorozawa, Saitama, Japan

[2] Department of Laboratory Medicine, National Defense Medical College, Tokorozawa, Saitama, Japan

[3] Department of Radiology, National Defense Medical College, Tokorozawa, Saitama, Japan

[4] Department of Urology, National Defense Medical College, Tokorozawa, Saitama, Japan

biopsy of suspicious lesions visualized on MP-MRI improves the rate of detection of clinically significant cancer, and MP-MRI may be used as a triage test to avoid unnecessary TRUS-biopsy in certain cases [6–10]. However, studies have also reported that MP-MRI fails to depict clinically significant cancers in a subset of patients [8, 11, 12]. One prospective multicenter study reported a 76% negative predictive value on MP-MRI for Grade Group 2 or higher cancers, suggesting that identification of some clinically significant prostate cancers were missed by the targeted biopsy [8]. Such missed lesions demand attention in order to improve upon the existing cancer screening procedure.

Although larger tumor size is one of the best predictors of detection on MP-MRI [13], some previous studies have assessed the relationship between the MRI-detectability and detailed histopathological patterns of prostate cancer [14–16]. In the recent studies that focused on the detectability of tumors with Gleason pattern 4, cribriform dominant tumors were less often detectable on MP-MRI than non-cribriform predominant tumors [14, 15]. However, this observation is controversial, given the study by Prendeville et al. [16], who reported that cribriform/intraductal pattern was significantly associated with a decreasing apparent diffusion coefficient value, thereby increasing MRI-detectability. On the other hand, studies that used quantified analysis of histological components in apparent diffusion coefficient restricted areas reported that the changes in volumes of cancer cells, stroma, and luminal spaces strongly correlated with apparent diffusion coefficient changes in prostate cancer [17–19]. However, these studies investigated only MRI-detectable lesions or a small number of ex vivo (i.e., post-radical prostatectomy) prostate specimens.

The present study reviewed histopathological findings in whole-mount sections of 59 radical prostatectomies performed for the treatment of invasive carcinoma. The cases had undergone preoperative MP-MRI and were standardized based on the tumor size on the radical prostatectomy specimen. A semi-automated imaging analysis was also performed to evaluate area fractions of the histological components, including cancer cells, stroma, and luminal spaces. Subsequently, MRI-detectability of prostate cancer was correlated with histopathological parameters, including Grade Group, subtypes of Gleason pattern 4, and area fractions of histological components of the tumor with the aim of determining the impact of these factors on the detectability of prostate cancer.

Materials and methods

Cases enrolled

The Ethics Committee of National Defense Medical College, Tokorozawa, Japan, approved this research protocol. The present study included 206 consecutive patients who had undergone MP-MRI, subsequent radical prostatectomy, and no neoadjuvant hormone therapy/radiotherapy between 2007 and 2018. Patients were excluded if the largest tumor diameter on the pathological specimen was <10 mm or more than 20 mm, to avoid bias in the size of the tumor on MP-MRI findings ($n = 144$). Following this, cases in which the largest tumors showed Grade Group 1 were excluded, because the tumors were pathologically insignificant ($n = 3$). Finally, a total of 59 prostate cancer cases met the criteria of the present study.

Histological evaluation

A total of 59 radical prostatectomy cases were retrieved from the files of the Department of Laboratory Medicine, National Defense Medical College. Two experienced surgical pathologists (KM and HT) reviewed the specimens to confirm the pathological findings. All radical prostatectomy specimens were processed using a standard protocol at our institution. The prostate specimens were placed in neutral buffered formalin and were allowed to fix for at least 24 h. Following formalin fixation, the specimens were inked to identify laterality. The apical and bladder neck margins were removed and radially sectioned in a cervical cone-like fashion. The seminal vesicles were amputated, sliced, and entirely submitted. The sections of the apex, bladder neck, and seminal vesicles (average: 13 sections) were submitted entirely as conventional small tissue blocks. The remainder of the specimen was cut transversely at 3–5 mm intervals from the apex to base and was submitted as whole-mount sections. Hematoxylin-eosin (H&E) stained slides were prepared from each paraffin block.

All slides were then marked with ink during microscopic evaluation to outline the boundaries of all foci of invasive carcinoma. A map of areas with invasive cancer was used to determine the size of the cancer (a largest diameter of the cancer focus on the sections). The tumors of which size was between 10 and 20 mm were included the following analysis. According to the updated criteria [1, 20], Gleason score and Grade Group of these cancer foci were evaluated. In Grade Group 2 and 3 (i.e., Gleason score 3+4 and 4+3, respectively) cases, percentage of Gleason pattern 4 was calculated in increments of 5%. In tumor foci showing Gleason pattern 4, predominant subtypes, including cribriform glands, fused glands, glomeruloid structures, and poorly formed glands, were observed.

Radiological evaluation

All examinations were performed on a 3T ($n = 54$) or 1.5T ($n = 5$) MRI scanner (Achieva 3T and Ingenia 1.5T, Philips Health-care, Eindhoven, The Netherlands). An

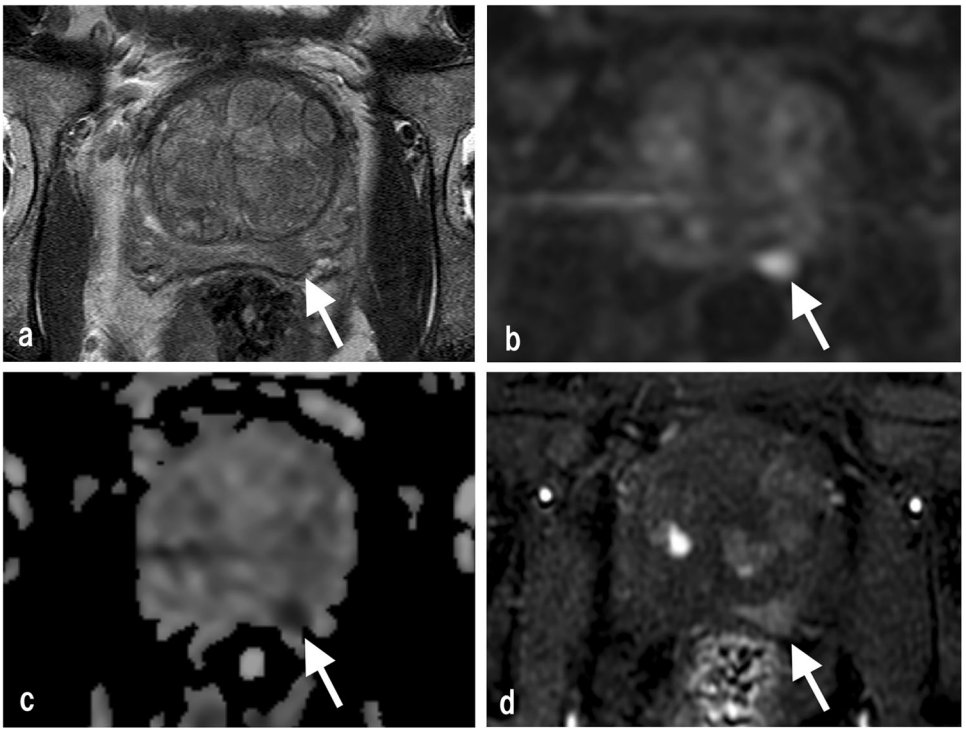

Fig. 1 Typical case of prostate cancer on multiparametric MRI. 63-year-old male patient with prostate cancer (prostate-specific antigen level, 5.6 ng/mL). A 12-mm nodule in the left peripheral zone (arrows) with hypointensity on T2-weighted image (**a**), hyperintensity on diffusion-weighted image (**b**), decreased apparent diffusion coefficient (**c**), and focal early enhancement on dynamic MRI (**d**) is seen, yielding a score of 4 on the Prostate Imaging Data Reporting System. Histopathology confirmed a tumor with Gleason score 4 + 4 in the corresponding area

intramuscular injection of 1 mg glucagon (Glucagon G Novo, Eisai, Woodcliff Lake, NJ) was administered before each examination. The examinations included axial and coronal T2-weighted imaging, axial diffusion-weighted imaging, and axial dynamic contrast-enhanced MRI. T2-weighted imaging was performed with repetition time (TR)/echo time (TE) of 4000–4848/70–90 ms, 3.5-mm slice thickness with 0.1-mm gap, 10 echo-train length, 512 × 260 matrices, and two excitations. Dynamic MRI was performed with TR/TE of 3.8/1.9 ms, flip angle of 15°, 3.0-mm slice thickness, and 240 × 194 matrices. In dynamic MRI, unenhanced baselines and 25, 60, and 180 s after bolus injection of 0.1 mmol/kg of gadodiamide hydrate (Omniscan, Daiichi Sankyo, Tokyo, Japan) or gadoteridol (Prohance, Braco-Eisai, Tokyo, Japan) were sequentially obtained. Diffusion-weighted imaging was performed with single-shot echo-planar imaging using three orthogonal diffusion sensitization directions, 3–10 *b*-values (from 0 up to 2000 s/mm^2), TR/TE of 4277–6499/40–69 ms, 3.5-mm slice thickness with 0.1-mm gap, 256 × 256 matrices, and sensitivity encoding of 2. Apparent diffusion coefficient maps were generated from diffusion-weighted imaging with *b*-values of 0 and 1000 s/mm^2. Of the 59 patients included, 22 and 37 patients underwent pre-biopsy and post-biopsy MRI scans, respectively. Reporting of MP-MRI scans was done by two experienced urologic radiologists (AM and HS). A 5-point Likert radiology reporting scale was used to designate prostates as highly unlikely (1), unlikely (2), equivocal (3), likely (4), and highly likely (5) to harbor clinically significant prostate cancer, which was based on the Prostate Imaging Data Reporting System (PIRADS) MP-MRI reporting consensus [21]. Representative images of MP-MRI are shown in Fig. 1. Each pathologically selected tumor on prostatectomy (i.e., tumor size ranging from 10 to 20 mm) was assigned a regional part (apex, mid, or base), sector (anterior or posterior), and laterality (left or right) in accordance with the PIRADS anatomical designations, and was paired with its corresponding MP-MRI image by matching the anatomical designations. A tumor focus on the radical prostatectomy specimen with a corresponding MP-MRI lesion with PIRADS score of 3 or greater was classified as "MRI-detectable". A tumor focus on the radical prostatectomy specimen that lacked a corresponding suspicious lesion (i.e., PIRADS score of 2 or less) with the same anatomical part was classified "MRI-undetectable".

Semi-automated image analysis

For each case, a representative slide was selected and cytokeratin (AE1/AE3) immunohistochemical staining was performed for semi-automated image analysis. Selected sections were deparaffinized in xylene and rehydrated in a graded alcohol series. Antigen retrieval was achieved by autoclaving (121 °C for 15 min) in 0.01 mol/L citrate buffer (pH 6.1), followed by cooling at room temperature. Endogenous peroxidase activity was blocked with 5% hydrogen peroxide. Each section was incubated overnight at 4 °C with

primary antibodies against cytokeratin (AE1/AE3, mouse monoclonal, dilution 1:100; Dako, Glostrup, Denmark). Subsequently, the slides were reacted with a dextran polymer reagent combined with secondary antibodies (Dako) for 1 h at room temperature. Specific antigen–antibody reactions were visualized with 0.2% diaminobenzidine tetrahydrochloride and hydrogen peroxide, and counterstaining was performed using Mayer's hematoxylin.

On each cytokeratin immunostaining section, five subimages with ×100 magnification (~10 mm^2 area) were obtained using a Keyence BZ-X710 microscope (Keyence, Osaka, Japan) and imported to the image analyzing software (BZ-X analyzer, Keyence). Semi-automated segmentation of the images into cancer cells, stroma, and luminal spaces was based on red, green, and blue color and brightness (Fig. 2). Following this, the mean area fraction of cancer cells, stroma, and luminal spaces was calculated for each tumor focus. As the grid method, based on the area of the tumor in histological slides, has been routinely used to estimate the volume of the tumor [22], the present study considered that the examined area fractions correlated with the relative volumes of cancer cells, stroma, and luminal spaces.

Statistical analyses

The association between MRI-detectability of cancer and clinicopathologic parameters including age of the patients, tumor location, tumor size, Grade Group, percentage of Gleason pattern 4, predominant subtype of Gleason pattern 4, time period between biopsy and MP-MRI, and the area fractions of the tumor components (i.e., cancer cells, stroma, and luminal spaces) were analyzed by the Chi square test, Fisher's exact test, or the Mann-Whitney *U* test. The multivariable analysis was performed using binomial logistic regression by including parameters that showed significant or marginal difference ($P < 0.10$) between MRI-detectable and MRI-undetectable cancers. Statistical calculations were performed using R software (version 3.4.2, R Core Team and Foundation for Statistical Computing, Vienna, Austria). Differences at $P < 0.05$ were considered statistically significant.

Results

In the 59 prostatectomy specimens analyzed in the present study, each presented with a cancer focus between 10 and 20 mm. No case showed two or more cancer foci, which conformed to the size criteria. Of the 59 foci of prostate cancer, 35 were MRI-detectable (i.e., PIRADS score of 3 or greater) and 24 were MRI-undetectable (i.e., PIRADS score of 2 or lesser).

Clinicopathological parameters of MRI-detectable and MRI-undetectable cancers are summarized in Table 1. The mean (median; range) age of the patients with MRI-detectable cancer was 67 years (67 years; 58–74 years) and with MRI-undetectable cancer was 68 years (69.5 years;

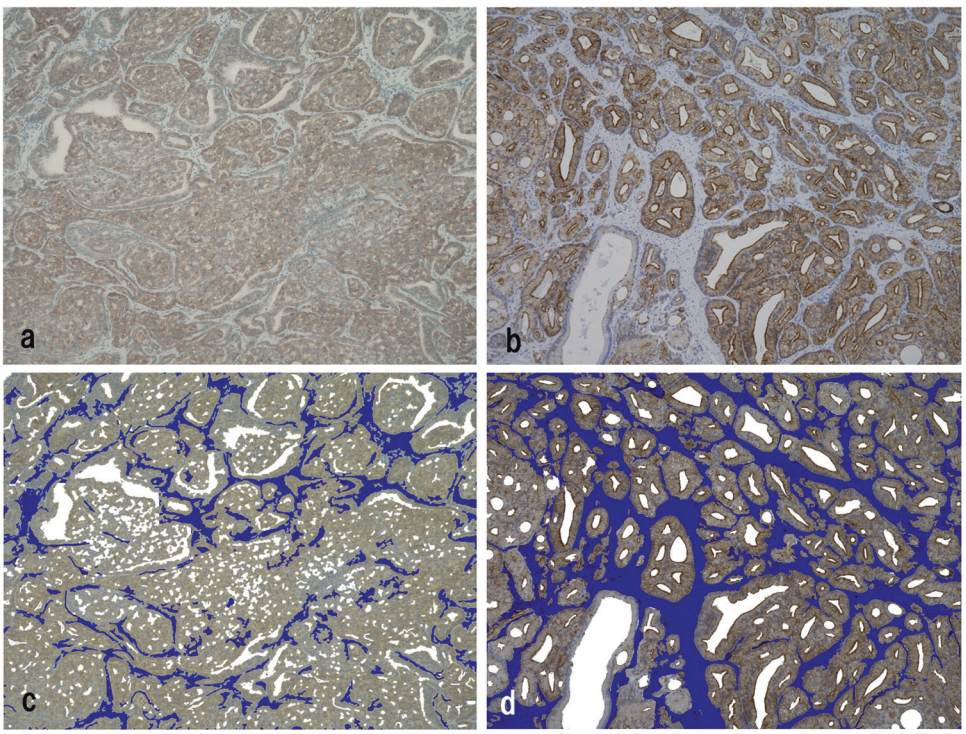

Fig. 2 Representative example of semi-automated analysis of histological images. **a**, **b** Immunohistochemical staining for cytokeratin AE1/AE3 highlighting cancer cells in (**a**) an MRI-detectable cancer and (**b**) an MRI-undetectable cancer, both of which show cribriform predominant growth. **c**, **d** Tissue components in (**c**) an MRI-detectable cancer and (**d**) an MRI-undetectable tumor are segmented into stroma (blue), luminal spaces (white), and cancer cells. Note a relatively higher area fraction of cancer cells and lower area fraction of stroma and luminal space in an MRI-detectable cancer as compared with an MRI-undetectable cancer. Immunoperoxidase stain, original magnification ×100

Table 1 Comparison of clinicopathological variables of MRI-detectable and undetectable cancers

Variables	MRI-detectability		*P* value
	Detectable ($n = 35$)	Undetectable ($n = 24$)	
Age (mean, year)	67	68	0.22
Location (PZ/TZ)	29/6	20/4	0.96
Tumor size (mean, mm)	13	14	0.26
Gleason Grade Group (2/3/4/5)	19/13/1/2	18/5/0/1	0.40
% Gleason pattern 4[a]	46.4	34.3	0.075
Predominant subtype of Gleason pattern 4 (cribriform/fused/glomeruloid/poorly formed)	6/12/3/14	3/6/0/15	0.25
Time period between biopsy and MRI[b] (mean, week)	6.0	6.3	0.69
Semiautomatic image analysis			
Cancer cells (mean, %)	60.9	42.7	<0.0001
Stroma (mean, %)	33.8	45.1	0.00089
Luminal space (mean, %)	5.2	12.2	<0.0001

MRI magnetic resonance imaging, *PZ* peripheral zone, *TZ* transition zone

[a]Only for tumors with Gleason score 7 (i.e., 3 + 4 or 4 + 3): 32 and 23 cases of MRI-detectable and undetectable cases, respectively

[b]Only for cases with post-biopsy MRI: 25 and 12 cases of MRI-detectable and undetectable cases, respectively

51–74 years). Twenty-nine and 6 MRI-detectable cancers and 20 and 4 MRI-undetectable cancers were located at peripheral zone and transition zone, respectively. The mean (median; range) tumor size of the patients with MRI-detectable cancer was 13 mm (14 mm; 10–18 mm) and with MRI-undetectable cancer was 14 mm (14 mm; 10–20 mm). No significant differences were observed in the mean age, location of the tumor, and the mean size of the tumor between cases with MRI-detectable cancer and MRI-undetectable cancer ($P = 0.22$, $P = 0.96$, and $P = 0.26$, respectively). The numbers of the prostate cancer stratified by Grade Group (2/3/4/5) were 19/13/1/2 on MRI-detectable cancers and 18/5/0/1 on MRI-undetectable cancers; and no statistically significant difference was observed between the two groups ($P = 0.40$). All cases with Grade Group 4 and Grade Group 5 were Gleason score 4 + 4 and Gleason score 4 + 5, respectively. The mean (median; range) percentages with Gleason pattern 4 in the total areas of cancer foci showing Grade Group 2 and Grade Group 3 were 46.4% (40%; 10–85%) on MRI-detectable cancers ($n = 32$) and 34.3% (30%; 10–90%) on MRI-undetectable cancers ($n = 23$). Marginal difference was observed in the percentage of Gleason pattern 4 between cases with MRI-detectable and MRI-undetectable cancers; however, the difference was not significant ($P = 0.075$). The numbers of the prostate cancer stratified by the predominant subtype of Gleason pattern 4 (cribriform glands/fused glands/glomeruloid structure/poorly formed glands) were 6/12/3/14 in MRI-detectable cancers and 3/6/0/15 in MRI-undetectable cancers; no statistically significant difference was observed between the two groups ($P = 0.25$). Sensitivities of MP-MRI for cribriform and non-cribriform predominant cancers (i.e., fused glands, glomeruloid structure, and poorly formed glands) were 66.7% (6/9) and 58.0% (29/50), respectively, with no statistically significant difference ($P = 0.63$). Of 37 tumor foci detected by the post-biopsy MP-MRI scan, 25 and 12 were MRI-detectable and MRI-undetectable, respectively. The mean (median; range) period between the biopsy and MP-MRI scan was 6.0 weeks (6 weeks; 4–10 weeks) on MRI-detectable cancers and 6.3 weeks (6.5 weeks; 4–10 weeks) in MRI-undetectable cancers, without statistically significant difference ($P = 0.69$).

The area fractions of the three tumor components (i.e., cancer cells, stroma, and luminal spaces) were evaluated by the semi-automated image analysis. The mean (median; range) area fraction of cancer cells was 60.9% (59%; 27–81%) in MRI-detectable cancers and 42.7% (42%; 20–64%) in MRI-undetectable cancers. As compared with MRI-undetectable cancers, MRI-detectable cancers showed significantly higher percentage of cancerous cells ($P < 0.0001$). The mean (median; range) area fractions of stroma and luminal spaces were 33.8% (36%; 12–72%) and 5.2% (4.8%; 0.73–16%) in MRI-detectable cancers and 45.1% (43.5%; 24–76%) and 12.2% (11%; 3.3–23%) in MRI-undetectable cancers, respectively. The mean area fractions of stroma and luminal space in MRI-undetectable cancers were significantly higher than those in MRI-detectable cancers ($P = 0.00089$ and $P < 0.0001$, respectively).

Next, a multivariable analysis using binomial logistic regression was conducted upon factors found to correlate

Table 2 Multivariable logistic regression analysis of clinicopathological variables of MRI-detectable and undetectable cancers

Variables	Odds ratio	95% CI	*P* value
% Gleason 4	1.67	−4.592 to 9.324	0.62
Cancer cells (mean, %)	23.02	11.20 to 43.15	0.0031
Luminal space (mean, %)	−64.04	−120.6 to −30.34	0.0035

CI confidence interval, *MRI* magnetic resonance imaging

with MRI-detectability of cancer (Table 2). The area fraction of stroma showed strong negative correlation with that of cancer cells (correlation coefficients = −0.92, $P < 0.0001$) (Spearman's correlation coefficient test), resulting in multicollinearity that could give rise to unreliable data. Hence, we performed the analysis upon exclusion of area fraction of stroma. Area fractions of cancer cells (odds ratio 23.02, 95% confidence interval 11.20–43.15, $P = 0.0031$) and luminal space (odds ratio −64.04, 95% confidence interval −120.06 to −30.34, $P = 0.0035$) demonstrated strong positive and negative correlation with MRI-detectability, respectively.

Discussion

Detailed evaluation of histopathological characteristics that affect MRI-detectability of prostate cancer is essential to recognize the limitation of MP-MRI and improve the diagnostic and therapeutic protocols for prostate cancer. In the present retrospective study, wherein the case cohort was standardized by the tumor size, no significant difference was observed in Grade Group, percentage of Gleason pattern 4, and predominant subtype of Gleason pattern 4 between MRI-detectable and MRI-undetectable cancers. Using semi-automated image analysis, significantly higher mean area fraction of cancer cells and lower mean area fractions of stroma and luminal spaces were observed in MRI-detectable than in MRI-undetectable cancers. In a multivariable analysis using logistic regression model, area fractions of cancer cells and luminal spaces positively and negatively correlated with MRI-detectability of cancer, respectively.

Cumulative evidence has suggested that the presence of cribriform architecture is a promising parameter for risk stratification of Gleason score 7 cancers [23–25]. In a large number of radical prostatectomies, where the index tumors had Gleason score 7, Kweldam et al. [23] reported that presence of cribriform growth was an adverse independent predictor for distant metastasis-free survival and disease-specific survival. Choy et al. [24] reported independent prognostic value of cribriform architecture on radical prostatectomy for biochemical recurrence. On the other hand, only a few studies have investigated the relationship between cribriform growth pattern and MRI-detectability of cancer. In a series of 22 patients who underwent radical prostatectomy, cribriform predominant tumors were less often visible on MP-MRI than non-cribriform predominant tumors [15]. However, a recent study using targeted biopsy combined with conventional TRUS-biopsy revealed controversial data of the strong relationship between cribriform pattern and a PIRADS score 5/decreasing apparent diffusion coefficient [16]. Moreover, in the present study, there is no statistically significant difference in sensitivities of MP-MRI for cribriform and non-cribriform predominant cancers. In addition to the differences in tissue sample as reference (biopsy vs. radical prostatectomy), sample size, and protocols of MP-MRI, it may be suggested that discrepancy may also arise due to the heterogeneous morphology of prostate cancer, even in the same histological subtype of Gleason pattern 4.

As a principle, the lower apparent diffusion coefficient in cancers than in normal tissues results from reduced water mobility, which has been commonly attributed to increased "cellularity" in various types of cancer including prostate cancer [26–29]. In the specific case of prostate tissue, there is considerable evidence that differences between the diffusion properties of the epithelium, stroma, and luminal space may affect apparent diffusion coefficient measured at clinical spatial resolution. Using 16T diffusion microimaging of fixed prostate tissue, one study group demonstrated that the glandular epithelium has lower apparent diffusion coefficient than stroma, which in turn has lower apparent diffusion coefficient than the luminal space [30, 31]. In addition, the group reported that high volume of epithelium and low volume of luminal spaces in cancers were more strongly associated with low apparent diffusion coefficient than high nuclear count/area measured by conventional cellularity metrics [17], which is in line with the results of the present study. However, the above-mentioned study performed only ex vivo analysis for measurement of apparent diffusion coefficient and data was obtained from a small sample of patients ($n = 14$). To the best of our knowledge, the present study is the first report comparing relative area fractions of cancerous histologic components (i.e., cancer cells, stroma, and luminal spaces) between in vivo MRI-detectable and MRI-undetectable cancers. The results indicate that differences in the relative volumes of the histological components are likely to be one of the major contributors to clinical MRI-detectability of prostate cancer. From this viewpoint, even in tumors categorized in the same histological pattern, identification of cancerous cribriform growth with larger luminal perforations and lesser number of cancerous cells may be missed on MP-MRI, and vice versa.

A positive aspect of the present study was that size of the tumor was adjusted between 10 and 20 mm. As it is well-known that tumor size is one of the strongest predictors of detection on MP-MRI [13, 14], avoiding bias related to size is important to evaluate an accurate association between histopathological features and MRI-detectability of cancer.

There are several limitations in the present study. First, there was some uncertainty in the precise match between the lesions detected on MP-MRI slices and the corresponding lesions defined in the histological slides; however, this problem is not specific to the method of the study. Another caveat of the present study was the strict delimitation of Gleason pattern 4 in the four subtypes. Although this subdivision reflects the categories described by the ISUP/WHO and was reviewed by two pathologists, partially poor interobserver reproducibility cannot be completely excluded. Finally, in a subset of cases, MP-MRI was performed post-TRUS-biopsy. According to a previous study [32], post-biopsy hemorrhage could hinder the accuracy of detection of cancer; therefore, waiting time of at least 4 weeks was followed in the present study before the MRI was performed after prostate biopsy. In addition, there was no significant difference in the time period from biopsy to MP-MRI scan between MRI-detectable and MRI-undetectable cancers.

In summary, the present data demonstrated that changes in the relative area fractions of cancer cells, stroma, and luminal spaces in prostate cancer, rather than conventional histological parameters including Grade Group, percentage of Gleason pattern 4, and predominant histological subtype of Gleason pattern 4, could be considered one of the best predictors in the in vivo MRI-detection of prostate cancer. It may be suggested that these findings reflect the fact that even in single subtype of Gleason pattern 4 (e.g., cribriform glands), marked morphological variations may be observed which affect MRI-detectability of the cancer. It is important to recognize this type of limitation of cancer detection by MP-MRI, and improvement is needed in the diagnostic approach, based on the histopathological features, to reduce the rate of missed diagnosis of clinically significant prostate cancer.

Acknowledgements The authors would like to thank Mr. Susumu Tominaga, Ms. Chinami Onuma, and Ms. Ru Hokari for their excellent technical assistance.

Compliance with ethical standards

Conflict of interest The authors declare that they have no conflict of interest.

References

1. Epstein JI, Egevad L, Amin MB, Delahunt B, Srigley JR, Humphrey PA. The 2014 International Society of Urological Pathology (ISUP) consensus conference on Gleason grading of prostatic carcinoma: definition of grading patterns and proposal for a new grading system. Am J Surg Pathol. 2016;40:244–52.
2. Miyamoto H, Hernandez DJ, Epstein JI. A pathological reassessment of organ-confined, Gleason score 6 prostatic adenocarcinomas that progress after radical prostatectomy. Hum Pathol. 2009;40:1693–8.
3. Wilt TJ, Jones KM, Barry MJ, Andriole GL, Culkin D, Wheeler T. Follow-up of prostatectomy versus observation for early prostate cancer. N Engl J Med. 2017;377:132–42.
4. Hassan O, Han M, Zhou A, Paulk A, Sun Y, Al-Harbi A, et al. Incidence of extraprostatic extension at radical prostatectomy with pure Gleason score 3+3=6 (Grade Group 1) cancer: implications for whether Gleason score 6 prostate cancer should be renamed "not cancer" and for selection criteria for active surveillance. J Urol. 2018;199:1482–7.
5. Heijnsdijk EA, der Kinderen A, Wever EM, Draisma G, Roobol MJ, de Koning HJ. Overdetection, overtreatment and costs in prostate-specific antigen screening for prostate cancer. Br J Cancer. 2009;101:1833–8.
6. Siddiqui MM, Rais-Bahrami S, Turkbey B, George AK, Rothwax J, Shakir N, et al. Comparison of MR/ultrasound fusion-guided biopsy with ultrasound-guided biopsy for the diagnosis of prostate cancer. JAMA. 2015;313:390–7.
7. Wegelin O, van Melick HHE, Hooft L, Bosch JLHR, Reitsma HB, Barentsz JO, et al. Comparing three different techniques for magnetic resonance imaging-targeted prostate biopsies: a systematic review of in-bore versus magnetic resonance imaging-transrectal ultrasound fusion versus cognitive registration. Is there a preferred technique? Eur Urol. 2017;71:517–31.
8. Ahmed HU, El-Shater Bosaily A, Brown LC, Gabe R, Kaplan R, Parmar MK, et al. Diagnostic accuracy of multi-parametric MRI and TRUS biopsy in prostate cancer (PROMIS): a paired validating confirmatory study. Lancet. 2017;389:815–22.
9. Kasivisvanathan V, Rannikko AS, Borghi M, Panebianco V, Mynderse LA, Vaarala MH, et al. MRI-targeted or standard biopsy for prostate-cancer diagnosis. N Engl J Med. 2018;378:1767–77.
10. Rouvière O, Puech P, Renard-Penna R, Claudon M, Roy C, Mège-Lechevallier F, et al. Use of prostate systematic and targeted biopsy on the basis of multiparametric MRI in biopsy-naive patients (MRI-FIRST): a prospective, multicentre, paired diagnostic study. Lancet Oncol. 2019;20:100–9.
11. de Rooij M, Hamoen EH, Witjes JA, Barentsz JO, Rovers MM. Accuracy of magnetic resonance imaging for local staging of prostate cancer: a diagnostic meta-analysis. Eur Urol. 2016;70:233–45.
12. Borofsky S, George AK, Gaur S, Bernardo M, Greer MD, Mertan FV, et al. What are we missing? False-negative cancers at multiparametric MR imaging of the prostate. Radiology. 2018;286:186–95.
13. Martorana E, Pirola GM, Scialpi M, Micali S, Iseppi A, Bonetti LR, et al. Lesion volume predicts prostate cancer risk and aggressiveness: validation of its value alone and matched with prostate imaging reporting and data system score. BJU Int. 2017;120:92–103.
14. Truong M, Hollenberg G, Weinberg E, Messing EM, Miyamoto H, Frye TP. Impact of Gleason subtype on prostate cancer detection using multiparametric magnetic resonance imaging: correlation with final histopathology. J Urol. 2017;198:316–21.

15. Truong M, Feng C, Hollenberg G, Weinberg E, Messing EM, Miyamoto H, et al. A comprehensive analysis of cribriform morphology on magnetic resonance imaging/ultrasound fusion biopsy correlated with radical prostatectomy specimens. J Urol. 2018;199:106–13.
16. Prendeville S, Gertner M, Maganti M, Pintilie M, Perlis N, Toi A, et al. Role of magnetic resonance imaging targeted biopsy in detection of prostate cancer harboring adverse pathological features of intraductal carcinoma and invasive cribriform carcinoma. J Urol. 2018;200:104–13.
17. Chatterjee A, Watson G, Myint E, Sved P, McEntee M, Bourne R. Changes in epithelium, stroma, and lumen space correlate more strongly with gleason pattern and are stronger predictors of prostate ADC changes than cellularity metrics. Radiology. 2015;277:751–62.
18. Helfrich O, Puech P, Betrouni N, Pinçon C, Ouzzane A, Rizk J, et al. Quantified analysis of histological components and architectural patterns of gleason grades in apparent diffusion coefficient restricted areas upon diffusion weighted MRI for peripheral or transition zone cancer locations. J Magn Reson Imaging. 2017;46:1786–96.
19. Langer DL, van der Kwast TH, Evans AJ, Plotkin A, Trachtenberg J, Wilson BC, et al. Prostate tissue composition and MR measurements: investigating the relationships between ADC, T2, K(trans), v(e), and corresponding histologic features. Radiology. 2010;255:485–94.
20. Epstein JI. An update of the Gleason grading system. J Urol. 2010;183:433–40.
21. Barentsz JO, Weinreb JC, Verma S, Thoeny HC, Tempany CM, Shtern F, et al. Synopsis of the PI-RADS v2 guidelines for multiparametric prostate magnetic resonance imaging and recommendations for use. Eur Urol. 2016;69:41–9.
22. Bostwick DG, Cheng L, Meiers I. Neoplasms of the prostate. In: Bostwick DG and Cheng L, editors. Urologic surgical pathology. Philadelphia, PA: Elsevier/Saunders; 2014. p. 408–531.
23. Kweldam CF, Wildhagen MF, Steyerberg EW, Bangma CH, van der Kwast TH, van Leenders GJ. Cribriform growth is highly predictive for postoperative metastasis and disease-specific death in Gleason score 7 prostate cancer. Mod Pathol. 2015;28:457–64.
24. Choy B, Pearce SM, Anderson BB, Shalhav AL, Zagaja G, Eggener SE, et al. Prognostic significance of percentage and architectural types of contemporary Gleason pattern 4 prostate cancer in radical prostatectomy. Am J Surg Pathol. 2016;40:1400–6.
25. Kweldam CF, Kümmerlin IP, Nieboer D, Steyerberg EW, Bangma CH, Incrocci L, et al. Presence of invasive cribriform or intraductal growth at biopsy outperforms percentage grade 4 in predicting outcome of Gleason score 3+4=7 prostate cancer. Mod Pathol. 2017;30:1126–32.
26. Gibbs P, Liney GP, Pickles MD, Zelhof B, Rodrigues G, Turnbull LW. Correlation of ADC and T2 measurements with cell density in prostate cancer at 3.0 Tesla. Invest Radio. 2009;44:572–6.
27. Zelhof B, Pickles M, Liney G, Gibbs P, Rodrigues G, Kraus S, et al. Correlation of diffusion-weighted magnetic resonance data with cellularity in prostate cancer. BJU Int. 2009;103:883–8.
28. Yoshikawa MI, Ohsumi S, Sugata S, Kataoka M, Takashima S, Mochizuki T, et al. Relation between cancer cellularity and apparent diffusion coefficient values using diffusion-weighted magnetic resonance imaging in breast cancer. Radiat Med. 2008;26:222–6.
29. Manenti G, Di Roma M, Mancino S, Bartolucci DA, Palmieri G, Mastrangeli R, et al. Malignant renal neoplasms: correlation between ADC values and cellularity in diffusion weighted magnetic resonance imaging at 3 T. Radio Med. 2008;113:199–213.
30. Bourne R, Kurniawan N, Cowin G, Sved P, Watson G. 16 T diffusion microimaging of fixed prostate tissue: preliminary findings. Magn Reson Med. 2011;66:244–7.
31. Bourne RM, Kurniawan N, Cowin G, Stait-Gardner T, Sved P, Watson G. Microscopic diffusivity compartmentation in formalin-fixed prostate tissue. Magn Reson Med. 2012;68:614–20.
32. Ko YH, Song PH, Moon KH, Jung HC, Cheon J, Sung DJ. The optimal timing of post-prostate biopsy magnetic resonance imaging to guide nerve-sparing surgery. Asian J Androl. 2014;16:280–4.